Conformational Dynamics of Hyaluronan in Solution. 2. Mode-Coupling Diffusion Approach to Oligomers

Sara Letardi,[†] Giovanni La Penna,[‡] Ester Chiessi,[§] Angelo Perico,[‡] and Attilio Cesàro*,[†]

Department of Biochemistry, Biophysics and Macromolecular Chemistry, University of Trieste, I-34127 Trieste, Italy; Istituto di Studi Chimico-fisici di Macromolecole Sintetiche e Naturali, National Research Council, via De Marini 6, I-16149 Genova, Italy; and Department of Chemistry Science and Technology, University of Rome "Tor Vergata", I-00133 Rome, Italy

Received July 13, 2001; Revised Manuscript Received October 8, 2001

ABSTRACT: A detailed study of structure and dynamics of hyaluronan oligomers $(UA)_4$ and $(UA)_2$ is presented. Recent advances in macromolecule diffusion theory are applied to second order in the mode-coupling expansion to derive second-rank time-correlation functions of the C−H vectors along the chains. The required equilibrium averages are approximated by time averages along an atomistic molecular dynamics simulation. The results are compared with experimental ^{13}C NMR relaxation parameters of different nuclei in the molecule. The pronounced structure in the relaxation pattern found in the experiments for $(UA)_4$ can be qualitatively interpreted in terms of rotational diffusion anisotropy with partially screened hydrodynamic interactions. Interresidue hydrogen bonds concerning the side chains are weak and do not have significant local effects while O5(i)−HO3/4(i + 1) hydrogen bonds can play a significant role in coupling conformational degrees of freedom with solvation. The implications of this study on the knowledge of the hyaluronan polymer structure and dynamics are addressed.

I. Introduction

Topological features of polysaccharide structure and dynamics are currently approached from several points of view (for a recent review see ref 1). In general, polysaccharides are better described by statistically pseudo-ordered or statistical random coil chains, the former residing on either intrachain or interchain interactions. Within this multiplicity of structural and conformational features, rules of thumb for chain topologies were assigned early to schematically ordered[2] or statistically averaged chains[3] and more recently to dynamic properties[4] of simple homoglycans.

These latter calculations of relaxation parameters based on diffusion theory and mode-coupling approach have been performed on different systems, ranging from synthetic polymers[5] to polysaccharides[4] and from proteins[6] to nucleic acids.[7] The method allows the calculation on a microscopic basis of every second-rank time correlation function (TCF) in the molecule once the configurational statistics have been modeled. Many approximations can be introduced in order to simplify this calculation in a macromolecule, but the necessary numerical model for the configuration weights has been found to be the most relevant assumption. In theory, every microscopic interaction can be included in the model for the statistics.

A particularly interesting aspect of glycans, like hyaluronan, is the effect of substituents on the backbone molecular conformation and dynamics. The presence of carboxyl groups in C6 in D-glucuronate residue (U), and *N*-acetamido group replacing O2 hydroxyl in residue 2-deoxy-2-acetamido-D-glucose (A), allows the formation of interresidue hydrogen bonds that can greatly modify local structure and mobility and, indirectly, change the solvation of the polymer segment.[8−10] The constraints due to medium-range interactions such as hydrogen bonds and long-range interactions between the polar or charged groups must be included in any realistic model of hyaluronan polymers. To experimentally monitor the structural and dynamical effects of such interactions, nuclear magnetic (NMR) relaxation measurements on oligomers and polymers in dilute water solution are widely performed. In the case of oligomers, due to the capabilities of high-field NMR instruments, almost every carbon chemical shift can be assigned up to the $(UA)_6$ oligomer and ^{13}C NMR relaxation can be monitored through the $R(C_z)$ and $R(C_{xy})$ relaxivity measurements at the applied magnetic field. The rates of single-exponential functions representing these decays, $R(C_z)$ and $R(C_{xy})$, are the inverse of the ^{13}C spin−lattice T_1 and spin−spin T_2 relaxation times, respectively, and are called relaxivities hereafter. Relaxivities contain information both on structure and molecular dynamics that are usually summarized in a set of order parameters and relaxation rates. Relaxivities are linear combinations of spectral densities that in turn are Fourier transform of second-rank time autocorrelation functions (TCFs) of inter-nuclear distance vectors. The interpretation of relaxivities is usually done by finding a set of parameters involved in the modeling of second-rank TCFs that fits the largest number of experimental data at hand. This approach is often limited by the many approximations introduced in the modeling in order to obtain a limited set of parameters and is greatly dependent on the experimental data set available.

Given the interest in addressing the study of possible networks of hydrogen bonds, electrostatic interactions, and solvation effects combined with short-range torsional potential occurring in hyaluronan oligomers, the

* Author for correspondence. E-mail: cesaro@univ.trieste.it.
† University of Trieste.
‡ National Research Council.
§ University of Rome "Tor Vergata".

10.1021/ma0112220 CCC: $22.00
Published on Web 12/04/2001

most affordable numerical technique to obtain the statistics is the molecular dynamics simulation algorithm (MD).[11] In this simulation, a deterministic trajectory of every configurational variable is acquired, and canonical ensemble statistical averages necessary to the diffusion theory are estimated by time averaging along the trajectory. The combination of MD simulations with diffusion theory gives a microscopic description of the NMR relaxation parameters for biopolymers, without any approximation concerning the separation of time scales.[12,13] Other approaches, such as direct calculation of local order parameters through computer simulations[14,15] or by normal mode based analysis[16] require some hypothesis about decoupling of overall rotation and internal motions.

It must be stressed that previous papers,[17−19] focusing on the comparison between MD simulations and NMR data for hyaluronan, did not involve a quantitative and straight derivation of NMR parameters from MD trajectories, but they paid attention to a qualitative explanation of chemical shifts, fitted order parameters, and distance constraints.

In this paper, we present a detailed interpretation of $R(C_z)$ ^{13}C relaxivities of different nuclei located in $(UA)_2$ and $(UA)_4$ oligomers measured in water solution at 300 K and at $\nu(^{13}C) = 75$ and 100 MHz. The connectivity of the studied oligomers is always $\{(\rightarrow 4)$-β-U$-(1\rightarrow 3)$-β-A$-(1\rightarrow)\}_n$, where U = D-glucuronate and A = 2-deoxy-2-acetamido-D-glucose.

The paper is organized as follows. In section II, the approximations in the solution of the diffusion equation within the mode-coupling approach are summarized. In section III, the preparation of starting configurations and the choice of the parameters regarding the MD simulation are described. In section IV, the convergence of the method in terms of hydrodynamic parameters (bead setup and hydrodynamic strength), trajectory length, and basis sets is presented. In section V, the molecular configurations explored by the MD trajectory are described in terms of a limited set of geometrical parameters, and the solvation state is analyzed. In section VI, a comparison with NMR relaxation experiments is made and discussed in terms of other related computed quantities describing local mobility. Section VII contains the concluding remarks, the implications of this study on the polymer behavior, and perspectives.

II. Diffusion Theory

The diffusion theory, applied to a dilute solution of macromolecules, treats the solvent hydrodynamically and adopts a detailed molecular model for the solute polymer in terms of beads (atoms or group of atoms) connected by real or virtual bonds diffusing in an atomistic potential.[20] In the mode-coupling matrix representation of the diffusion equation, the potential has no particular role, but is contained in the statistical averages necessary to the theory.[5] The beads are represented as points in position $\mathbf{r}_i$, characterized by their friction coefficients $\zeta_i = 6\pi\eta a_i$, with η the solvent viscosity (0.001 Pa s for water at 300 K). The Stokes radii a_i were calculated here by using the accessible surface area (ASA) method with a zero probe radius by summing the surfaces of each group constituent, according to the procedure outlined in the literature.[21] For such relatively small molecules, like the hyaluronan oligomers up to $n = 6$, a detailed model where each methylene, methyl, hydroxyl, carboxyl, amino, and carboxy group is represented separately as a single bead can be treated (Table 1). The ether oxygen atoms (O5 and O1) are treated as single beads in order to include in the diffusive model correlation between the bonds in the pyranose rings and the bonds connecting two monomers.

Table 1. Stokes Radii (pm) of Beads in Models I and II (for Model III See Text)

Model I

	center	surface atoms	Stokes radius
U	C1	C1, H1	93
	O1	O1	73
	O5	O5	74
	C5	C5, H5	100
	C6	C6, O61, O62	179
	C4	C4, H4	89 (110 in U1)
	O4 (in U1)	O4, HO4	110
	C3	C3, H3	110
	O3	O3, HO3	110
	C2	C2, H2	80
	O2	O2, HO2	80
A	C1	C1, H1	93 (110 in A4)
	O1	O1 (H1 in A4)	73 (110 in A4)
	O5	O5	74
	C5	C5, H5	92
	C6	C6, H61, H62, O6, HO6	185
	C4	C4, H4	110
	O4	O4, HO4	110
	C3	C3, H3	80
	C2	C2, H2	90
	N2	N2, H22	83
	C22	C22, O22	134
	C72	C72, HM1, HM2, HM3	177

Model II

	center	ASA contributions of groups in model I	Stokes radius
U	C4 (in U1)	C4+O4	151
	C3	C3+O3	148
	C2	C2+O2	111
A	C4	C4+O4	147
	C1 (in A4)	C1+O1	161

In the following, the mode-coupling diffusion approach to describe the dynamics in polymer solutions is briefly summarized.[22,23] Given a polymer of N_a beads of friction coefficients ζ_i and coordinates $\mathbf{r}_i$, $i = 1, ..., N_a$, connected by N_b bonds ($\mathbf{l}_i$, $i = 1, ..., N_b$), the dynamics of the macromolecule described by the variables $\mathbf{l}_i$, is governed by the operator L, adjoined to the diffusion Smoluchowski operator D

$$\frac{\partial \mathbf{l}}{\partial t} = L\mathbf{l}; \quad L = \sum_{i,j=1}^{N_a} [\nabla_i \cdot \mathbf{D}_{i,j} \cdot \nabla_j - (\nabla_i U/k_B T) \cdot \mathbf{D}_{i,j} \cdot \nabla_j] \quad (1)$$

where $\mathbf{l}$ is the $3N_b$ dimension vector containing all the bonds, $\mathbf{D}$ the diffusion tensor, U the bead potential energy, k_B the Boltzmann constant, and T the temperature.

By expansion of the conditional probability (the solution to the Smoluchowski equation) in a complete set of eigenfunctions of L, the time autocorrelation function (TCF) of any coordinate-dependent dynamic variable with zero average $f(t)$, may be expressed in the standard form

$$\langle f(t)f(0)\rangle = \sum_i \langle f|\psi_i\rangle\langle\psi_i|f\rangle \exp(-\lambda_i t) \quad (2)$$

where λ_i and ψ_i are the eigenvalues and the normalized eigenfunctions of the operator L.

By representing ψ_i in a set of basis functions $\Phi = \{\phi_m, m = 1, ..., M\}$

$$\psi_i = \sum_{m=1}^{M} C_{m,i}\phi_m \tag{3}$$

the diffusion eigenvalue equation may be written in matrix form

$$\mathbf{FC} = \mathbf{SC}\Lambda \tag{4}$$

with Λ the diagonal matrix with the eigenvalues λ_m as the diagonal elements, **C** the eigenvector matrix of coefficients $C_{i,m}$, **S** the metric matrix

$$S_{ij} = \langle\phi_i\phi_j\rangle \tag{5}$$

and **F** the equilibrium force matrix

$$F_{ij} = -\langle\phi_i|L\phi_j\rangle = \sum_{m,n=1}^{N_a} \langle(\nabla_m\phi_i)\cdot\mathbf{D}_{mn}\cdot(\nabla_n\phi_i)\rangle \tag{6}$$

where

$$\begin{aligned} \boldsymbol{D}_{ij} &= D_i\mathbf{H}_{ij} \\ \mathbf{H}_{ij} &= \mathbf{1}\delta_{ij} + \alpha\zeta_i\mathbf{T}_{ij}(1 - \delta_{ij}) \\ \mathbf{T}_{ij} &= (8\pi\,\eta\,r_{ij})^{-1}\,[\mathbf{1} + \mathbf{r}_{ij}\,\mathbf{r}_{ij}/{r_{ij}}^2] \end{aligned} \tag{7}$$

with **H** and **T** representing the hydrodynamic interaction matrix and Oseen tensor, respectively.

$$D_i = k_B T/\zeta_i \tag{8}$$

is the diffusion coefficient of each bead and η the solvent viscosity.

The factor α in the hydrodynamic interaction of eq 7 is a parameter whose values are often restricted to the range $\alpha < 1.0$ so as to maintain a positive definite **H**, while $\alpha = 1.0$ corresponds to the full interaction strength related to the specific choice of friction coefficients.

The ensemble equilibrium averages, indicated within brackets in the above equations, are calculated as

$$\langle a|b\rangle = \int P_{eq}(\mathbf{r})\, a(\mathbf{r})\, b(\mathbf{r})\, d\mathbf{r} \tag{9}$$

with $P_{eq}(\mathbf{r})$ the equilibrium distribution function depending on the potential energy U. In the following, the equilibrium statistical averages will be calculated by time averaging along a MD trajectory for the full atomistic model of the given molecule in explicit water (see next section). As the eigenfunctions ψ_i are orthonormalized, the coefficient matrix **C** should satisfy the normalization equation

$$\mathbf{C}^T\mathbf{SC} = 1 \tag{10}$$

Accurate approximations to the TCFs evaluation are obtained by taking basis functions in the basis set built with increasing power of the variables, bond vectors or their linear combinations, in the spirit of the mode-coupling theory.[22,23]

First and second-order basis sets, which must be given in the proper irreducible tensorial form, are therefore, for second-rank functions, bilinear and tetralinear, respectively, in the bond variables.

The relationship between NMR experimentally measured magnetization decay rates and TCFs are given by[24,25]

$$\begin{pmatrix} R(C_z) \\ R(C_{xy}) \\ R(H_z \rightarrow C_z) \end{pmatrix} = \begin{pmatrix} 0 & d & (3d + c) & 0 & 6d \\ \dfrac{(6d + 2c)}{3} & \dfrac{d}{2} & \dfrac{(3d + c)}{2} & 3d & 3d \\ 0 & -d & 0 & 0 & 6d \end{pmatrix} \begin{pmatrix} J(0) \\ J(\omega_I - \omega_S) \\ J(\omega_S) \\ J(\omega_I) \\ J(\omega_I + \omega_S) \end{pmatrix} \tag{11}$$

where

$$d = \frac{1}{20}\left(\frac{\gamma_S\gamma_I\hbar}{4\pi\epsilon_0 c^2}\left\langle\frac{1}{{r_{SI}}^6}\right\rangle\right)^2 \tag{12}$$

$$c = \frac{1}{15}(\varpi_S\delta)^2 \tag{13}$$

S and I refer to two unlike spins, in this case ^{13}C and ^{1}H respectively, γ is the gyromagnetic ratio, r_{SI} is the carbon-proton distance, and δ is the chemical shift anisotropy (dimensionless) of the observed carbon nucleus (−40 ppm for all C−H bonds in the polysaccharides here considered). The spectral density $J(\omega)$ is the Fourier transform of a TCF that is described below. In the case studied here the two nuclei are always bonded through a covalent bond that is allowed to stretch in the statistics: therefore, the average of $1/r^6$ in eq 12 was computed along the MD trajectory. The three nuclear magnetic relaxation rates (relaxivities hereafter) obtained through eq 11 deal with three different magnetization components. The NMR data that will be compared with calculations are $R(C_z)$, available for almost every C nucleus in the $(UA)_4$ and $(UA)_2$ molecules.

Finally

$$J(\omega) = 2\int_0^\infty \cos(\omega t)TCF(t)\, dt \tag{14}$$

are the spectral densities required to compute the rates in eq 11 and the time autocorrelation functions are of the for

$$TCF(t) = \sum_{M=-2}^{2} \langle[D^{(2)*}_{M,0}(\Omega(t))][D^{(2)}_{M,0}(\Omega(0))]\rangle = \langle P_2(\cos(\beta(t))\rangle \tag{15}$$

where $D^{(2)}_{M,0}$ are irreducible spherical tensors,[26] Ω is the orientation of the given C−H vector, P_2 is the Legendre polynomial of order 2, and β is the angle that the C−H vector spans in time t.

Given the above equations, relating the $R(C_z)$ parameters derived by the experiment to the second-rank TCFs describing the relaxation of the C−H vectors, we can finally introduce a molecular description of these relaxations.

As f of eq 2 is a second-rank irreducible spherical function of a molecular vector, the projections $\langle f|\phi_m\rangle$ on the basis elements ϕ_m are nonzero if and only if ϕ_m is a

second-rank function. Therefore, the ϕ_m basis functions must be constructed as second-rank functions. As a consequence, the **S** and **F** matrix elements are averages of products of second-rank irreducible spherical tensors. The evaluation of these elements is made simply by computing the scalar components (rotational invariants) contained in the products of second-rank functions in the matrix elements.[23]

Summarizing, along the MD trajectory the rotational invariant of the **S** and **F** matrix elements (eqs 5 and 6) and of the $\langle f|\phi_m\rangle$ projections are calculated, the matrix eq 4 is solved, and eqs 2 and 3 are used to compute TCFs, one for each of the C−H monitored bonds. Once the second rank TCFs are computed, they can be Fourier transformed to the spectral densities (eq 14).

We summarize below an efficient procedure for finding a reduced basis set to compute accurate tensor time correlation functions.[23] The first step amounts to solving the diffusion equation with a basis that is linear in the bonds in order to get the first order dynamics for a vector function:

$$\{l_{i,x}\}\ i = 1, ..., N_b \tag{16}$$

The first-order solution is obtained by the diagonalization of eq 4, which gives the first-order vector eigenfunctions $m_{i,x}$:

$$m_{i,x} = \sum_{j=1}^{N_b} C_{j,i} l_{j,x} \tag{17}$$

For quasi-rigid structures, ignoring the modes of higher rates means neglecting very small contributions to the TCFs that correspond to fast decaying exponential terms related to these modes. This is evident for the first order and is still valid for higher orders due to the combined effect of the products of fast decaying exponential terms. Therefore, we can select a reduced basis set, generally built with the e modes of lowest rates of eq 16, with e equal to the dimensionality d of the space or a value much lower than N_b. For second-rank functions, a reduced second-order basis set RM2-II can be generated in the proper irreducible tensorial form. Once e first-order vector modes are chosen, this second-order basis set contains $e(e + 1)/2$ second powers and $[e(e + 1)/2]^2$ fourth powers of the modes.

As observed above, this second-order basis set RM2-II is expected to give a good approximation to the dynamics of fluctuating structures because it gives in the rigid limit the "exact" rotational dynamics.

III. Simulation Setup

Starting from the sugar $(AU)_4$ coordinates in the unit cell of hyaluronan from X-ray fiber diffraction data, taken from the protein data bank,[27] the program CHARMm[28] was used to generate a $(UA)_4$ structure and to merge it in a water box. Since the $(AU)_4$ structure has a $\{(\rightarrow 3)$-β-A$-(1\rightarrow 4)$-β-U$-(1\rightarrow)\}_n$ connectivity, the first A residue was removed and a final A residue was constructed to obtain the $\{(\rightarrow 4)$-β-U$-(1\rightarrow 3)$-β-A$-(1\rightarrow)\}_n$ oligomer. The coordinates for the last residue were constructed using the information contained in the CHARMm internal coordinates database and setting the ϕ and ψ dihedral angles of the last glycosidic linkage equal to 60 and 0°, respectively, to be consistent with the other glycosidic linkages in the starting crystallographic configuration and with the results of previous simulations.[8−10,17,29] After the addition of the hydrogen atoms according to the CHARMm internal database, the molecule was placed in the center of a 4.2 nm side cubic box and immerged in a box of 2106 TIP3P water molecules equilibrated at a density of 0.985 g/cm^3 and temperature of 298 K.[30] The side was chosen in order to be consistent with the oligomer experimental concentration of 5% in weight necessary for the NMR experiments. Any water molecule overlapping the solute was removed.

The obtained configuration was used as the starting configuration for the MD simulation performed using the ORAC 4.0 program[31,32] with the CHARMm forcefield. Calculations were carried out using the velocity−Verlet algorithm in the multiple time-step formulation[33] in order to include all the degrees of freedom in the dynamics.[32] This allowed an integration step size of $^1/_4$ fs for the intramolecular interaction (bonds stretching and angle bendings) and an eight times larger time step (2 fs) for the longer-range interactions (dihedral torsions, electrostatic, and Lennard-Jones interactions).

Periodic boundary conditions were used to overcome finite-size effects, and Lennard-Jones interactions were smoothly switched off between 0.8 and 0.9 nm. Electrostatics was calculated using the smooth particle-mesh Ewald method with $\alpha = 4.3$ nm^{-1} and a grid size of 0.1 nm.[34] The starting configuration was first heated to 100 K rescaling the velocities for 50 ps. This stage was followed by 100 ps of NVE dynamics and this equilibration procedure was repeated at 200 and 300 K. A further heating stage of 150 ps (during which velocities were rescaled) was followed by a trajectory of 2 ns that was acquired in the NVE statistical ensemble. Configurations were saved every 0.5 ps and used to compute the configuration-dependent quantities whose averages are needed in eqs 2, 5, 6, and 9. Total energy was -60.8 ± 0.3 MJ/mol, and the temperature was 304 ± 3 K. Since the different components of the potential energy do not show any significant drift or jump, all of the saved configurations were used for the following analysis.

To construct the $(UA)_2$ structure, the last four residues were removed from the starting $(UA)_4$ configuration. Following the previous procedure, this molecule was immerged in a 2.4 nm side cubic box filled with 356 TIP3P water molecules and the same simulation protocol was applied to heat the system. A trajectory of 1 ns was acquired in the same NVE micro-canonical statistical ensemble.

Since the most interesting discussion deals with the $(UA)_4$ oligomer that spans about one pitch of the helical structure shown by crystallographic data, in the following section the results for the $(UA)_4$ oligomer are presented and those concerning $(UA)_2$ are used for the interpretation of the longer oligomer.

IV. Choice of Hydrodynamic Parameters

Friction points were placed on a selected group of heavy atoms in the solute molecule (see the three schematic representations shown in Figure 1). The most detailed model used here to describe polysaccharides (model I hereafter) assumes as friction points the groups in Table 1, i.e., centered on almost every heavy atom in the molecule. Model II is obtained by collecting in one friction point some of the hydroxy−methylene groups in model I and summing the corresponding ASAs. Finally, model III consists of two beads for each residue, each bead having half the surface of the belonging

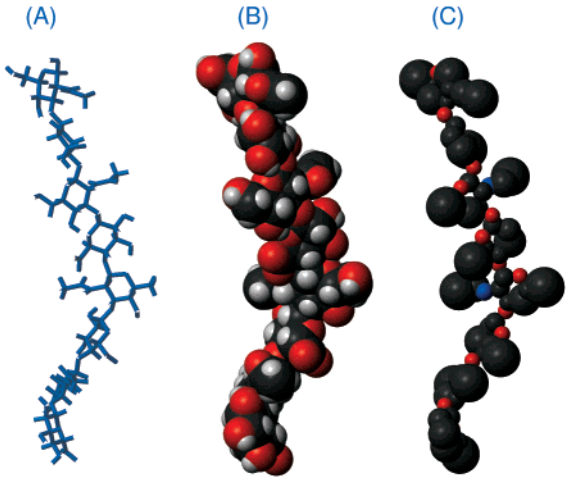

Figure 1. Schematic representation of the $(UA)_4$ oligomer in the first snapshot of the MD trajectory: stick representation of covalent bonds (A), spheres with the force-field Lennard-Jones' radii (B), and spheres in the diffusive model II with the hydrodynamic radii assigned by computing the accessible surface area of the group constituents (C).

residue: for U residues, the beads are centered in C4 and C1 and have equal Stokes radii of 228 pm, while those for A residues are centered in C3 and C1 with radii equal to 278 pm. To compare these different bead representations, Figure 2 shows $P_2(t)$ correlation times and $R(C_z)$ for each of the experimentally monitored C nuclei at 75 MHz.[19] Results for C6(A) are averaged over the two C−H bonds. A hydrodynamic strength α of 0.25 was used for the reasons that will be explained later. Since the experimental rates at 75 MHz are about 4.5 s^{-1}, Figure 2B shows that model III does not represent the rotational second-rank rates of the diffusion propagator well, as it is achieved by both model II and model I. The addition of a few friction points on the hydroxyl oxygen going from model II to model I does not change significantly either the average $R(C_z)$ or the pattern of data within the different nuclei (dynamic pattern hereafter). It must be pointed out that the average $R(C_z)$ data can, in theory, be increased either by decreasing the hydrodynamic strength or by increasing the size of the beads: in this case, even with $\alpha = 0$, with model III it is not possible to match experiments at 75 MHz while the choice of the criterion to build reduced sets of beads from the atomic ones has been found to be reasonable for similar systems. The reason for the big difference between the two more detailed models and model III lies in the much larger anisotropy in the five rotational second-rank rates (the five lowest rates) in the latter model: even though the lowest rate changes only slightly (0.37 GHz in model III compared to 0.25 GHz in model I), the highest rate is about 1 order of magnitude larger (18 GHz compared with 2.4 GHz). Moreover, in model III the two highest rotational rates are of the same magnitude as the further "internal" rates. In other words, the linear array of beads in model III is not sufficiently thick to represent the rotational dynamics of the $(UA)_4$ oligomer and at least some of the friction of the beads representing the pyranose rings must be explicitly included in the model. In the following, model II is used for all the calculations as an optimum compromise between a detailed hydrodynamic description and a reduced number of beads to save computer time. This model has $N_a = 75$ (8 beads on U, 11 beads on A, 10 beads on A4) and $N_b = 74$.

Before going into more details about the diffusive model, it is worth checking the convergence of the dynamic pattern with the MD trajectory length. In Figure 3, the results obtained by increasing the length of 0.5 ns are shown: it can be observed that while the dynamic pattern is almost stable in the central residues after 1 ns, the convergence of terminal residues requires at least 1.5 ns. The slow convergence of dynamic patterns obtained by diffusion theory in terms of deterministic simulations has already been pointed out[6] and raises many questions on the reliability of MD simulations in the importance sampling of configurations even in the case of such small molecules. In the following, the MD trajectory of 1.5 ns is used for all the calculations.

As already carried out for other systems, the effect of the number of basis set elements on the dynamic pattern has been measured increasing the e parameter in the construction of the RM2-II basis set from $e = 3$ (the minimum requested by the maximum correlation approximation), that means 42 basis functions, to $e = 5$, i.e., 240 basis functions. In Figure 4, the dynamic pattern at 75 MHz shows that the effect of increasing e is small and does not change essentially the structure of the plot that appears to be slightly shifted upward by increasing the number of basis functions. In the following calculations, a value of $e = 3$ has always been used.

To check the sensitivity of the comparison with experimental results to the hydrodynamic strength, in Figure 5 the correlation times and the dynamic pattern $R(C_z)$ at four values of α are plotted. It is interesting to notice that even if the correlation times are strongly affected by α (Figure 5A), the dynamic pattern, in particular the average of $R(C_z)$, is only slightly sensitive to this parameter (Figure 5B). In theory, the largest possible value for α must be chosen when dealing with water solution, but the optimal choice of hydrodynamic strength is definitely led by comparison with experiments (see the following subsection), particularly on similar molecules of different size or experiments collected at different ^{13}C frequencies. However, the major effect of hydrodynamic strength in the case of the $(UA)_4$ oligomer is in the flattening of the full screened ($\alpha = 0$) dynamic pattern structure by increasing α. The comparison between parts A and B of Figure 5 shows that the dynamic pattern obtained with $\alpha = 0$ resembles the behavior of the correlation times along the chain more than in the cases where $\alpha > 0$. By inspection of the second-rank rates obtained with different α, it can be observed that the effect of the hydrodynamic strength is not trivial: the lowest rate goes from 0.13 to 0.48 GHz changing α from 0 to 0.7; the other four rotational rates are only doubled, the second rate going from 0.66 to 1.3 GHz for instance; the sixth rate, as an example of the effect on the internal rates, goes from 12 to 55 GHz, with a relative effect of the same size as the first rate. The increase in the first rate with α almost explains the decrease of the average correlation time. The small internal rates that are achieved with $\alpha = 0$ may be responsible for the structure in the dynamic pattern within each residue, but this is not in effect at the experimental frequencies as will be seen later.

Finally, it must be noticed that the use of a different hydrodynamic tensor, such as the Rotne−Prager tensor,[35] does not change either the dynamic pattern or the correlation times up to $\alpha = 1$ (data not shown).

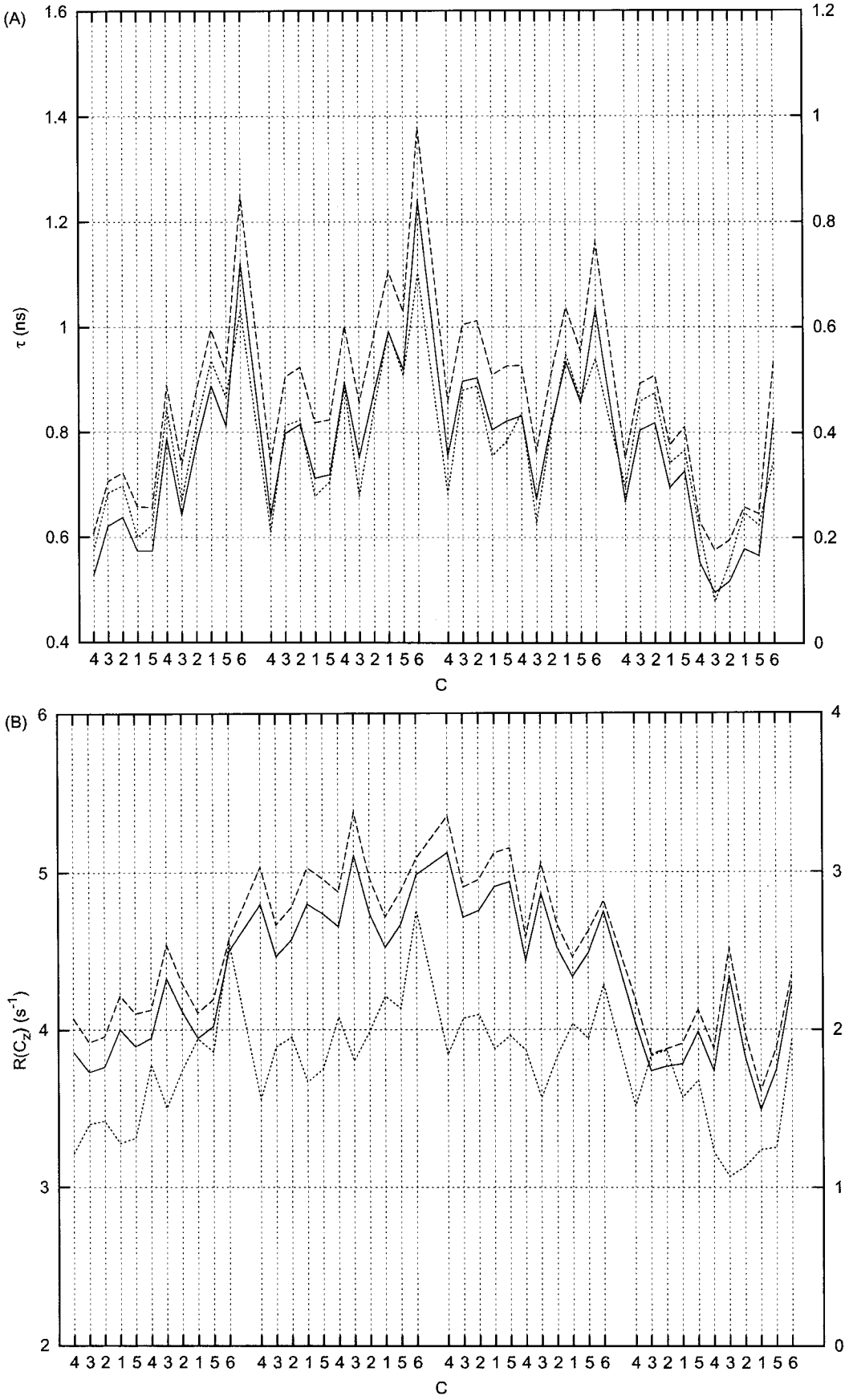

Figure 2. Comparison between different bead models for $(UA)_4$ oligomer with $\alpha = 0.25$ and $e = 3$: correlation times of $P_2(t)$ (A) and ^{13}C relaxivity at 75 MHz (B) for C−H bonds along the chain for model I (solid line, left y axis), model II (dashed line, left *y* axis), and model III (dotted line, right *y* axis). Above and in the following figures, carbon atoms are identified according to the standard nomenclature and oligosaccharide structure starts with nonreducing unit (U) at left, ending with the reducing unit (A) at right. Carbon atom numbering in abscissa (here and following figures) starts from C4 in counterclockwise order, by grouping UA units. This order is purely arbitrary and does not imply any dynamic correlation.

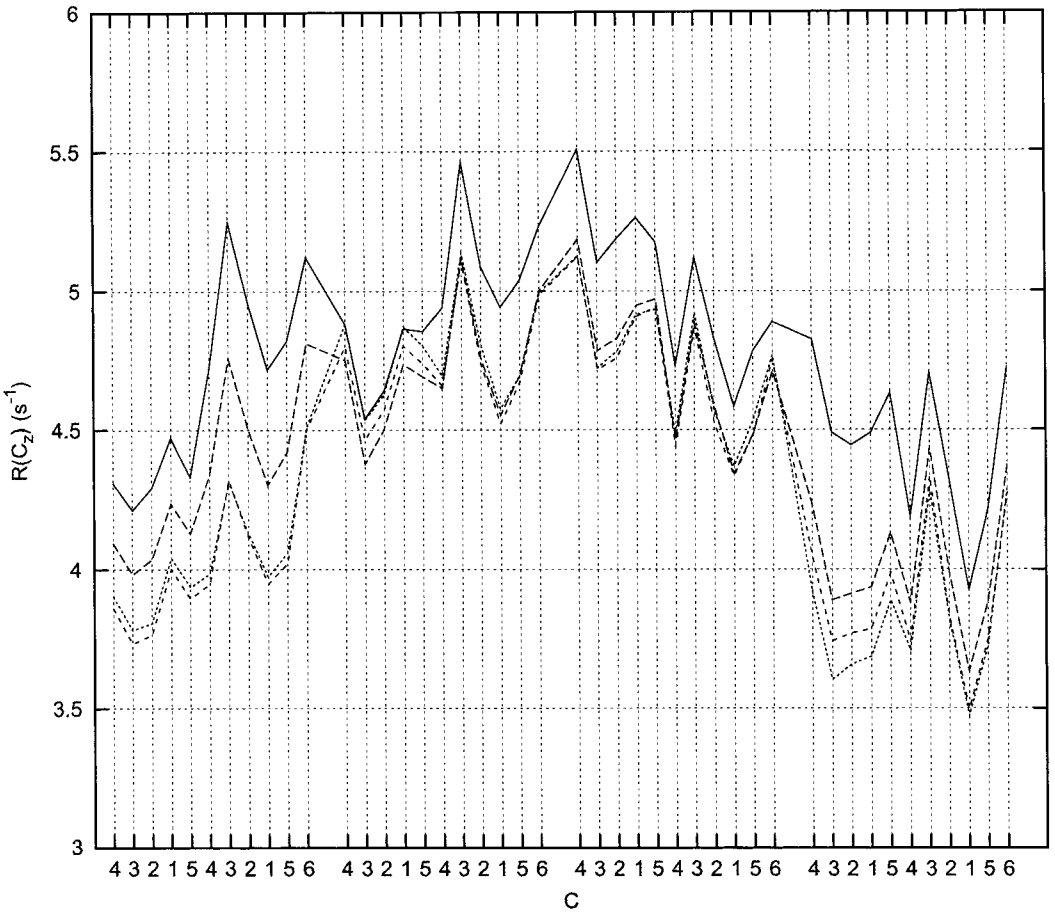

Figure 3. Comparison between relaxivities at 75 MHz for the same carbon of Figure 2 calculated with model II, $\alpha = 0.25$, $e = 3$ and MD trajectories of different lengths: 0.5 (solid line), 1 (long-dashed line), 1.5 (short-dashed line) and 2 ns (dotted line).

V. Configuration Statistics

In this section, a few parameters describing the configurations that are most represented in the MD statistics are summarized in order to give an idea of what the average molecule is, disregarding the deterministic time-evolution included in the simulation and retaining the statistical weights computed by the microcanonical MD trajectory of 1.5 ns. The shape of the molecule is governed by four sets of geometrical parameters: the ϕ and ψ dihedral angles that are relatively free to rotate; the conformation of sugar pyranose rings, monitored through the pucker Q and φ_2 angles;[36] a set of intra- and interresidue distances determined by NMR experiments that are sensitive to both the previous conformational parameters;[17] a set of distances that summarize the possible hydrogen bonds or salt bridges between side chains.

In Table 2 the averages of ϕ and ψ dihedral angles in $(UA)_4$ are shown (errors are root-mean-square deviations along the sampled configurations). These data, with the exception of the last ψ glycosidic linkage, are in agreement with the crystallographic input configuration[27] and with previous simulations of hyaluronan, even if in different force-field.[17] The last ψ angle was affected by a jump during the equilibration. The Q angle in the eight pyranose rings was found to be about 36°, that is twice the value found in the crystallographic structure (17°): this means that the pyranose rings are in flattened $^4C_1$ configurations.[36] The direction of the distortion can be found through the φ_2 angle, but this has been found spread in the whole domain, with broad peaks centered at 90° for U1, U2, and U3 residues and 120° for A1, A2, and A3 residues, compared to the 130° angle found in the crystallographic structure. The distances monitored by NMR experiments and published in the literature[17] are reported in Table 3: the agreement of the MD trajectory and NMR constraints is very good.

These three data sets confirm that as far as the experimental crystallographic and NMR evidence is concerned the trajectory represents well a fluctuating molecule with an average shape close to the starting left-hand helical pitch of the crystallographic structure.

A first graphical search of possible strong interactions that may be responsible for the stability of the pitch in $(UA)_4$ did not reveal interactions where the side chains are directly involved. The hydrogen bond between the N2 amidic hydrogen of A(i) and the O6 of U($i + 1$) present in the crystallographic structure is broken during thermalization. On the other hand, strong hydrogen bonds between HO3(U)/HO4(A)(i)−O5($i - 1$) have been found, with distances of 0.26 ± 0.05 and 0.22 ± 0.06 nm, respectively. This hydrogen bond is also present in the crystallographic structure. Apart from these stable interactions, there is no direct evidence of any particular intramolecular electrostatic interaction that may give specific contributions to the potential energy of the molecule.

To mimic the presence of a possible counterion shell, the neutralization of the carboxylic group of U in the force-field has been adopted, therefore avoiding the use of explicit counterions in the simulation. The consequent breaking of the hydrogen bond on the U side-chain initially present in the crystallographic structure can

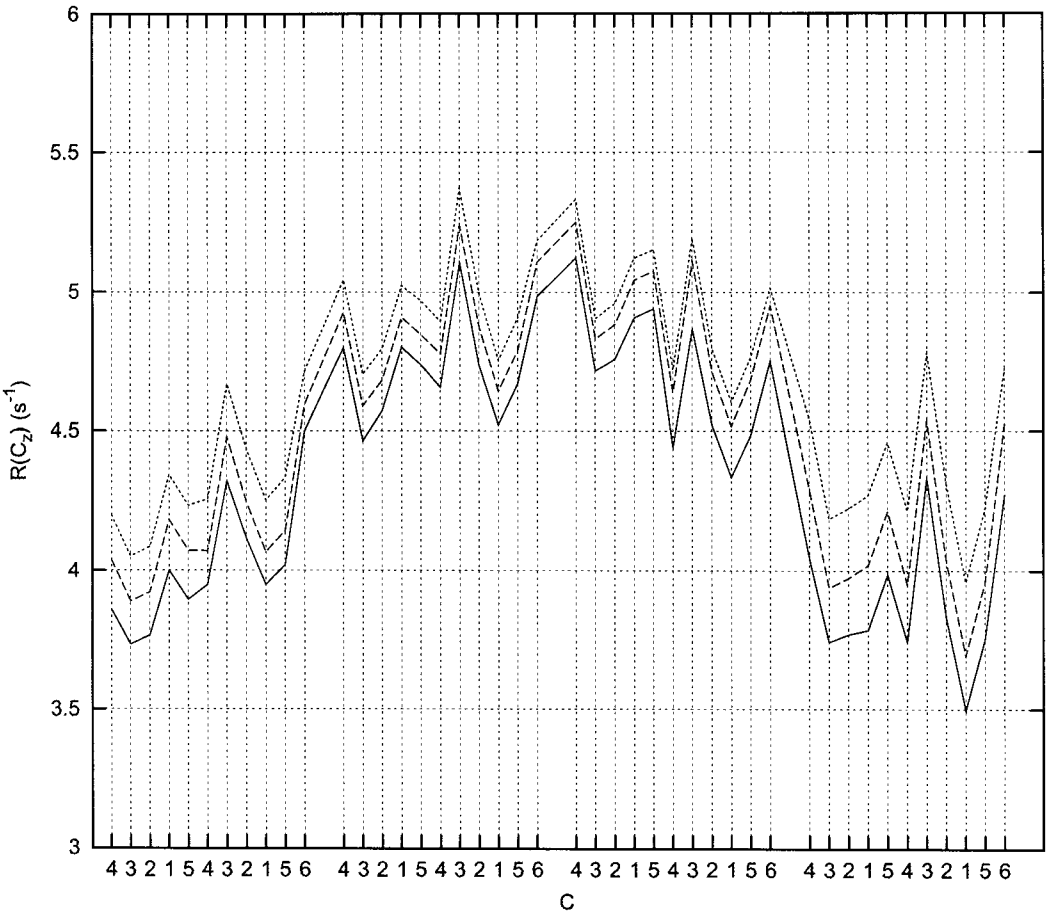

Figure 4. Comparison between the same relaxivities of Figure 2B calculated with model II, $\alpha = 0.25$ and different values of *e*: $e = 3$ (solid line), $e = 4$ (dashed line), and $e = 5$ (dotted line).

reduce the rigidity of the oligomer. On the other hand, the strength of the O5($i - 1$)−HO4/3(A/U i) hydrogen bond is influenced by conformational states that are not sampled by the present MD trajectory, possibly due to the finite trajectory. The persistence of this latter hydrogen bond makes the oligomer more rigid. These two effects partially cancel each other, and a correct molecular rigidity can be still well represented by the model.

To analyze the possible role of localized water molecules, the number of water molecules in the vicinity of each solute atom was computed. A cutoff distance of 0.35 nm between the water oxygen atom and any of the solute atoms was chosen as a closeness criterion for any water molecule. In Figure 6, this number is reported along with the solute atom labels. Only numbers greater than 1 are displayed and the label of carbon atoms—hydrogen, oxygen, hydroxyl, carbonyl and amino atoms bonded to each labeled carbon—follow on the right of each carbon. The pattern can be summarized as follows. The atoms belonging to the hydroxy-methylene groups on C2(U), C6(A) and on the terminal C1(A) are the most solvated; O2(U) is solvated like O3(U) only in the initial U residue; the U carboxyl atoms are not solvated as much as the previous set of atoms, mainly because the charges have been neutralized in the force-field; the methyl atoms in A are on average more solvated than the carboxyl groups; ring O5 oxygen atoms, hydrogen bonded with HO3/4 of the next residue in the chain, have less than one water molecule nearby. The high solvation of C6 hydroxy-methylene and C7 methyl groups in A residues can be explained with their embedding in the solvent, as both groups are at the end of side chains. The pattern of high solvation on the main chain hydroxyl groups in U with respect to A is mainly explained by the presence of two side chains in A with respect to the single carboxyl group in U. It is worth noticing that the strong hydrogen bond between O5(A_i) and its first neighbor HO3(U_{i+1}) in the chain, constrains O6(A_i) and O3(U_{i+1}) to face the solvent on the same side of the solute, while the hydrogen bond between O5(U_i) and HO4(A_{i+1}) forces O3(U_i) and O6(A_{i+1}) to be on opposite sides. Therefore, the hydrogen bond exposed by the MD simulation is strongly correlated to the solvation pattern and can indirectly influence the hydrodynamic properties of the oligomer and of the polymer.

Finally, comparing part A of Figure 6 with part B, it can be observed that the solvation patterns of $(UA)_4$ and $(UA)_2$ are almost the same.

In the following analysis, the numbering of residues begins from the nonreducing end and the atom names are the same of the PDB file containing the crystallographic coordinates (3HYA), except the glycosidic linkage oxygen that is referred as O1 instead of O3 in A and O4 in U (see Figure 1).

VI. Comparison with Experiments

In Figure 7, the calculated dynamic patterns of $R(C_z)$ at 75 and 100 MHz are compared with the available experiments for the $(UA)_4$ oligomer.[18,19] For this comparison, model II and the 1.5 ns MD trajectory were used with $\alpha = 0.25$. The choice of this latter parameter

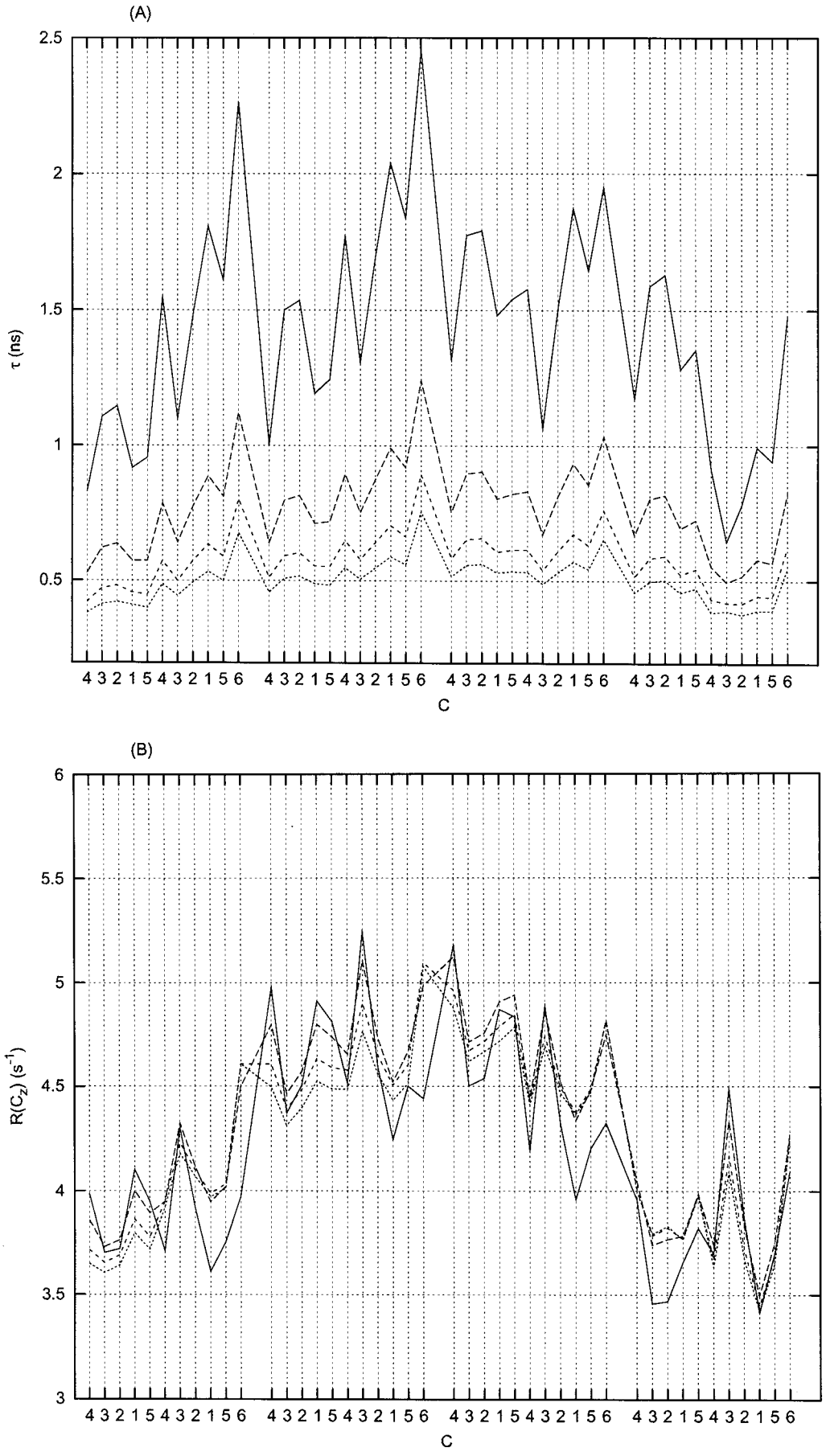

Figure 5. Comparison between $P_2(t)$ correlation times (A) and relaxivities at 75 MHz (B) calculated with model II, $e = 3$, and different values for α: $\alpha = 0$ (solid line), $\alpha = 0.25$ (long-dashed line), $\alpha = 0.5$ (short-dashed line), and $\alpha = 0.75$ (dotted line).

Table 2. Glycosidic ϕ and ψ Dihedral Angles (deg) Computed for $(UA)_4$ Compared to the Values in the Starting Configuration, with Root Mean Square Deviations within Parentheses

residue pair	dihedral	MD averaged	starting structure
U1−A1	ϕ	45 (10)	66
	ψ	7 (12)	−6
A1−U2	ϕ	38 (12)	41
	ψ	−9 (17)	10
U2−A2	ϕ	45 (10)	68
	ψ	6 (11)	2
A2−U3	ϕ	41 (12)	37
	ψ	−8 (16)	9
U3−A3	ϕ	43 (10)	66
	ψ	8 (13)	−6
A3−U4	ϕ	42 (11)	41
	ψ	−6 (17)	10
U4−A4	ϕ	47 (10)	57
	ψ	151 (12)	142

Table 3. Set of Selected Distances (nm) Computed for $(UA)_4$ Compared to NMR Derived Distances with Root Mean Square Deviations within Parentheses

atom pair	residue pair	MD av	NMR[a]
H1−H22	A1−A1	0.27 (0.02)	
	A2−A2	0.27 (0.02)	0.27
	A3−A3	0.27 (0.02)	
	A4−A4	0.26 (0.02)	
H1−H22	U1−A1	0.27 (0.03)	
	U2−A2	0.27 (0.03)	0.25
	U3−A3	0.27 (0.04)	
	U4−A4	0.28 (0.04)	
H1−H3	U1−A1	0.23 (0.02)	
	U2−A2	0.23 (0.02)	0.20
	U3−A3	0.23 (0.02)	
	U4−A4	0.23 (0.02)	
H1−H4	A1−U2	0.22 (0.02)	
	A2−U3	0.23 (0.02)	0.21
	A3−U4	0.23 (0.02)	
H1−H3	U1−U1	0.27 (0.02)	
	U2−U2	0.27 (0.02)	0.26
	U3−U3	0.27 (0.02)	
	U4−U4	0.27 (0.02)	
H1−H5	U1−U1	0.24 (0.02)	
	U2−U2	0.24 (0.02)	0.24
	U3−U3	0.24 (0.02)	
	U4−U4	0.24 (0.02)	

[a] Reference 13 in text.

was dictated by comparison with the results obtained for $(UA)_2$. Model II and the 1 ns MD trajectory obtained for $(UA)_2$ were used with different hydrodynamic strengths in order to find the best α value able to match the data sets of both oligomers (Figure 8), keeping in mind that for $(UA)_4$ the effect of increasing α is slight on the experimentally monitored $R(C_z)$ parameter (see Figure 5B). By this procedure, a value of $\alpha = 0.25$ has been derived: this value is approximately the same used for polysaccharides in applications of first-order diffusion theory. The effects on the dynamic pattern obtained by increasing the order of the mode-coupling expansion and the hydrodynamic strength are expected to partially cancel one an other. The compensation between these two effects, as well as those related to the actual molecular flexibility, must be verified for every system using the largest amount of data at hand.

It is worth making several comments on experimental data presented in Figure 7. The different experimental techniques used to obtain $R(C_z)$ at the two different ^{13}C resonance frequencies, with gated decoupling and inversion recovery for 100 and 75 MHz, respectively, show that, in addition to the error contained in each data set, a systematic error on those relaxation parameters must be considered, because the differences are too large to be motivated by the small frequency difference.[37]

Two aspects are common to the two data sets: first, both the data sets display, on average, lower relaxivities close to the nonreducing oligomer termination; second, a marked structure within the pyranose rings belonging to the central residues of the oligomer is shown in both cases, even if they are definitely different. The "gated decoupling" method chosen by Cavalieri et al.[18] gives a lower accuracy for relaxivity determination than the "inversion recovery" method used by Cowman et al.[19] The choice of Cavalieri et al. can only be justified by the need of the optimization of measurement times of the full set of parameters by sacrificing a more rigorous approach for the determination of relaxation parameters. Taking into account that the agreement between calculated and measured dynamic patterns is qualitatively good for the data collected at 75 MHz and the observations above about the "gated decoupling" technique regarding the data at 100 MHz, any further comparison is limited to the former data set.

Observing Figure 7B, experimental data can be analyzed in terms of an asymmetric bell shape, with terminations showing lower values than the central residues, modulated by a structure within each residue, where C3 and C1 show larger values than the other carbon nuclei. The same structure is not present in the $(UA)_2$ data (Figure 8), where almost all the behavior of the terminal residues of $(UA)_4$ is retained and there are not enough central residues. Note that in $(UA)_4$ the difference in relaxivity between central and terminal residues is represented, but not the lower values in the nonreducing termination. The structure of the dynamic pattern within each residue is partially represented, but less pronounced while the larger relaxivity for C3 and C1 with respect to other nuclei has not been captured. The major question, therefore, is why most of the structural parameters agree with the available experimental information while the dynamic pattern is only qualitatively reproduced. The following discussion is devoted to possible explanations of this discrepancy.

Assuming that the five lowest rotational rates are found in the correct range, it must be noticed that the relaxation parameters for the $(UA)_4$ oligomer are not simply related to the correlation times of the $P_2(t)$ TCF governing the second-rank orientational dynamics of the related C−H bond. This holds because no low-rate exponential term in each TCF has a leading role and a grouping of the exponential functions cannot be performed as in isotropic cases. For the same reason, relaxivities cannot be described through a unique order parameter defined along with the segregation of rotational and internal rates that could be performed for isotropic molecules.[6] This complication has already been pointed out for anisotropic systems in the frame of the "model free" approach and for this reason the application of this latter procedure usually provides a set of many correlated parameters. In the mode-coupling approach such complications are included in the model, mainly through the many amplitudes projecting each bond onto the second-rank diffusive propagator, but still remains the problem of a rationale for the many functions brought into the description of TCFs. Bearing in mind the brief description of the geometry of con-

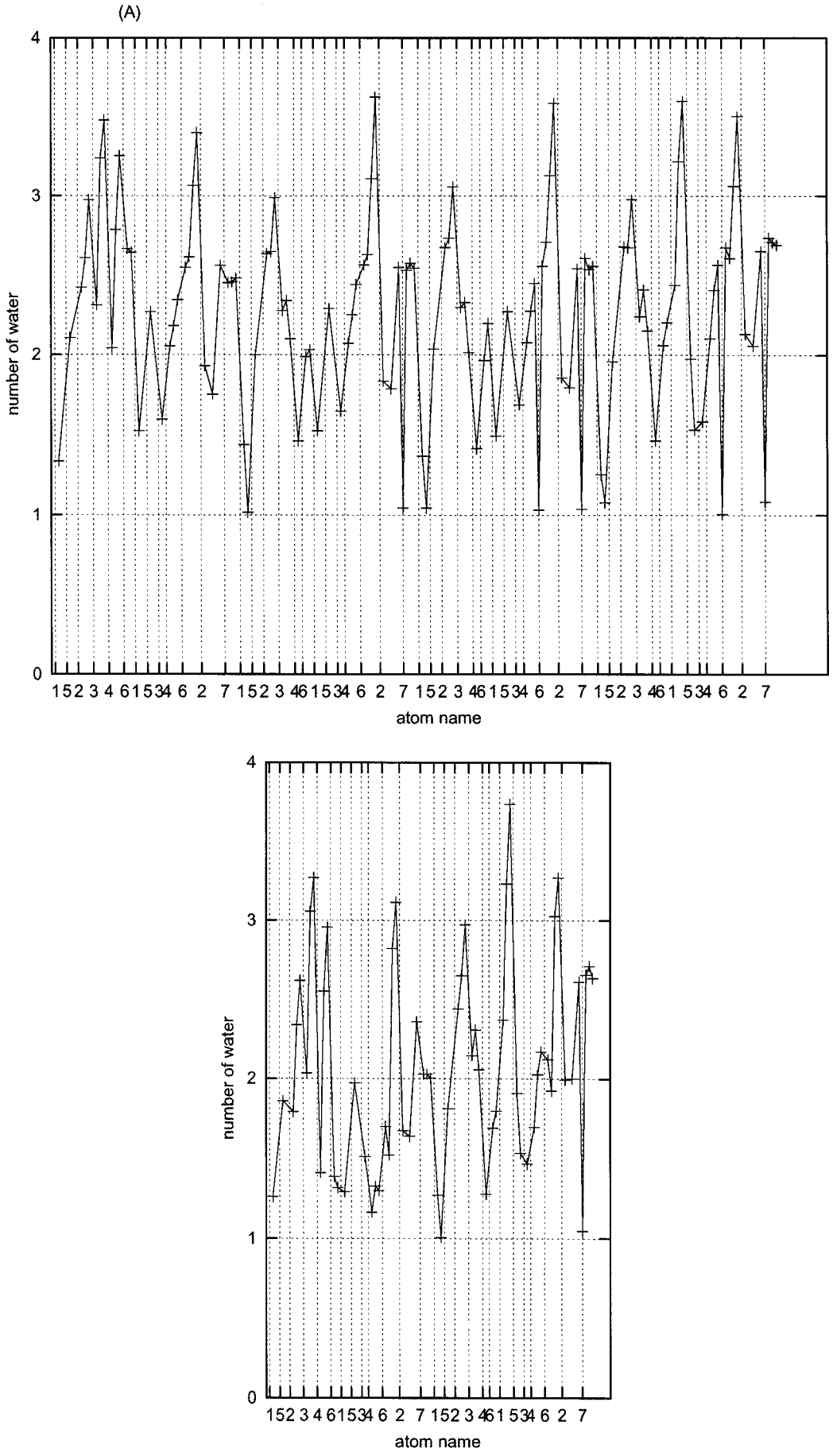

Figure 6. Number of water molecules within the distance of 0.35 nm from each solute atom as a function of the solute atom in the molecule.

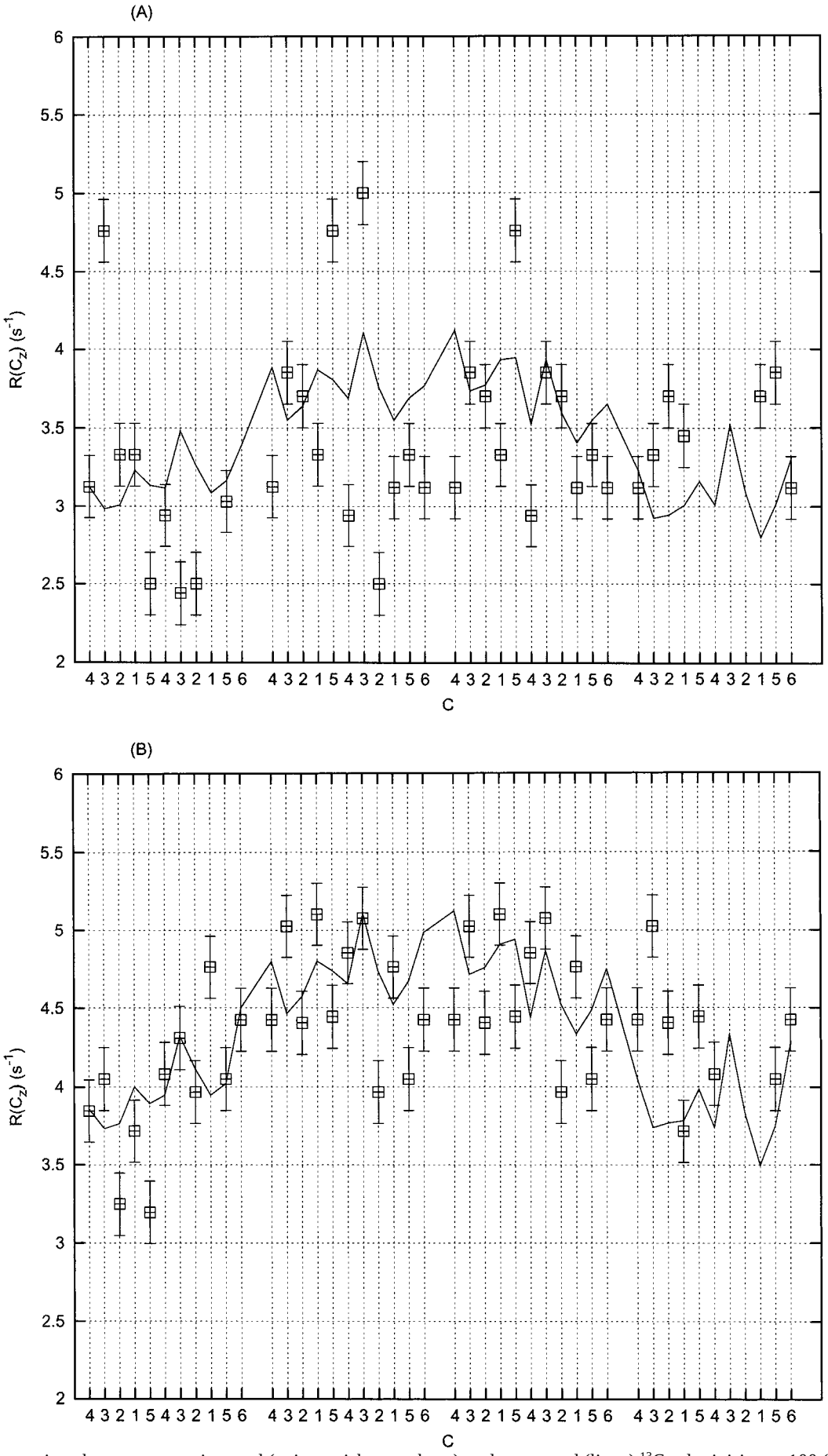

Figure 7. Comparison between experimental (points with error bars) and computed (lines) ^{13}C relaxivities at 100 (A, ref 14) and 75 MHz (B, ref 15) for $(UA)_4$ oligomer.

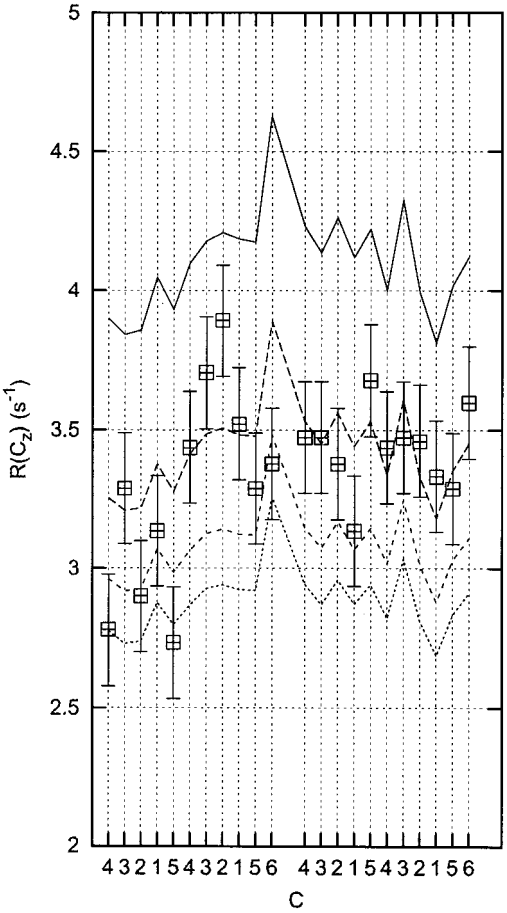

Figure 8. Comparison between experimental ^{13}C relaxivities at 75 MHz for the $(UA)_2$ oligomer[15] and values calculated with model II, $e = 3$, and different values of α: α = 0 (solid line), α = 0.25 (long-dashed line), α = 0.5 (short-dashed line), and α = 0.7 (dotted line).

figurations included in the statistics (see Section V), a few experiments below make the diffusive picture clearer and attempt to test possible sources of structure in the relaxation pattern.

The first question is as follows: Can the loss of structure in the computed dynamic pattern with respect to experiments be due to the loss of structure and to the disorder collected in the MD trajectory? The answer can be given through a simple experiment: the application of the mode-coupling diffusion theory to the starting structure that is close to the crystallographic one. For a rigid molecule constituted by friction points, the mode-coupling result coincides with the diffusion theory of rigid bodies. In Figure 9, the dynamic pattern at 75 MHz is shown at four different α values, 0, 0.25, 0.5 and 0.75. As expected, the average $R(C_z)$ is larger than in the flexible case because of both the change of lowest "rotational" rates and amplitudes and the possible contributions of higher-rate modes (representing the internal flexibility) in this latter case. However, the comparison of Figure 9 with Figure 5B reveals a strong effect of flexibility even in the central residues, which are more rigid. It is interesting to notice that hydrodynamic strength does not greatly affect the dynamic pattern of the rigid configuration; instead, an increase of α beyond 0.25 shifts all the values uniformly. Therefore, the effect of hydrodynamic strength is different in the rigid oligomer from that in the flexible case. This is because of the very different rotational rates in the two cases that make the relaxivities in the rigid molecule more reminiscent of the behavior of correlation times, which appear to be shifted in both cases (Figure 5A and data not shown for the rigid starting structure). For instance, if the lowest rate for the rigid molecule with $\alpha = 0.25$ is very similar to the corresponding rate in the flexible molecule (0.33 compared to 0.29 GHz), the other four rates in the rigid molecule are more than 10 times smaller than in the flexible molecule. The rigid molecule appears much thicker and therefore more isotropic than the average flexible molecule, and this is revealed by the corresponding relaxivities.

Nevertheless, to explain the variation of about half a unit in relaxivity within each residue shown by experiments, it must be noticed that even in the rigid molecule, data within each pyranose ring are very similar, while a marked difference can be observed between U and A residues, with the exception of the U3−A3 pair. Therefore, it does not seem reasonable to explain the structure shown by the experiments in terms of a peculiar orientation of C3−H3 and C1−H1 bonds with respect to the other C−H bonds in the same pyranose ring.

A second question can be raised about the role of internal rates in the structure of dynamic pattern: Are these modes important? It is possible to artificially increase the internal rates to infinite, keeping only the contribution of amplitudes and rates of the five lowest-rate modes in describing the required TCFs. The result for the $(UA)_4$ oligomer is that the dynamic patterns are almost identical (data not shown) with and without the high-rate modes (the internal modes mentioned above) for all the values of hydrodynamic strength, thus confirming that the computed dynamic pattern is, in this frequency range, governed by the anisotropic rotational diffusion.

A possible explanation of the disagreement of calculations with the large experimental relaxivity of C3 and C1 in each ring may be that the force-field is not able to sample the amplitudes of each bond in the five rotational modes. It appears unlikely that a different force-field can show the same regularity of the experiments, assuming that the experiments are sufficiently accurate.

VII. Conclusions

In this paper, recent advances in diffusion theory have been applied to the study of the molecular dynamics of two hyaluronan oligomers, $(UA)_4$ and $(UA)_2$, the former representing one pitch of the 3-fold helix structure of the polymer in the fiber. Average statistical quantities have been obtained by a MD trajectory in an atomistic potential; results are in agreement with structural information obtained by experiments and represent the wobbling of the molecule about a stable conformation.

The ^{13}C NMR $R(C_z)$ relaxivities have been compared with two available experimental data sets, which however display differences that have been attributed to the different techniques used by the authors.[14,15] A good qualitative agreement between the calculations for the two oligomers with the experiments obtained by the "inversion recovery" technique is emphasized.

It is noteworthy that the diffusive model allows the identification of the most important contributions to the dynamics. It has been found that anisotropy of rotational diffusion, quantified through the five lowest second-rank rates and the related amplitudes, is es-

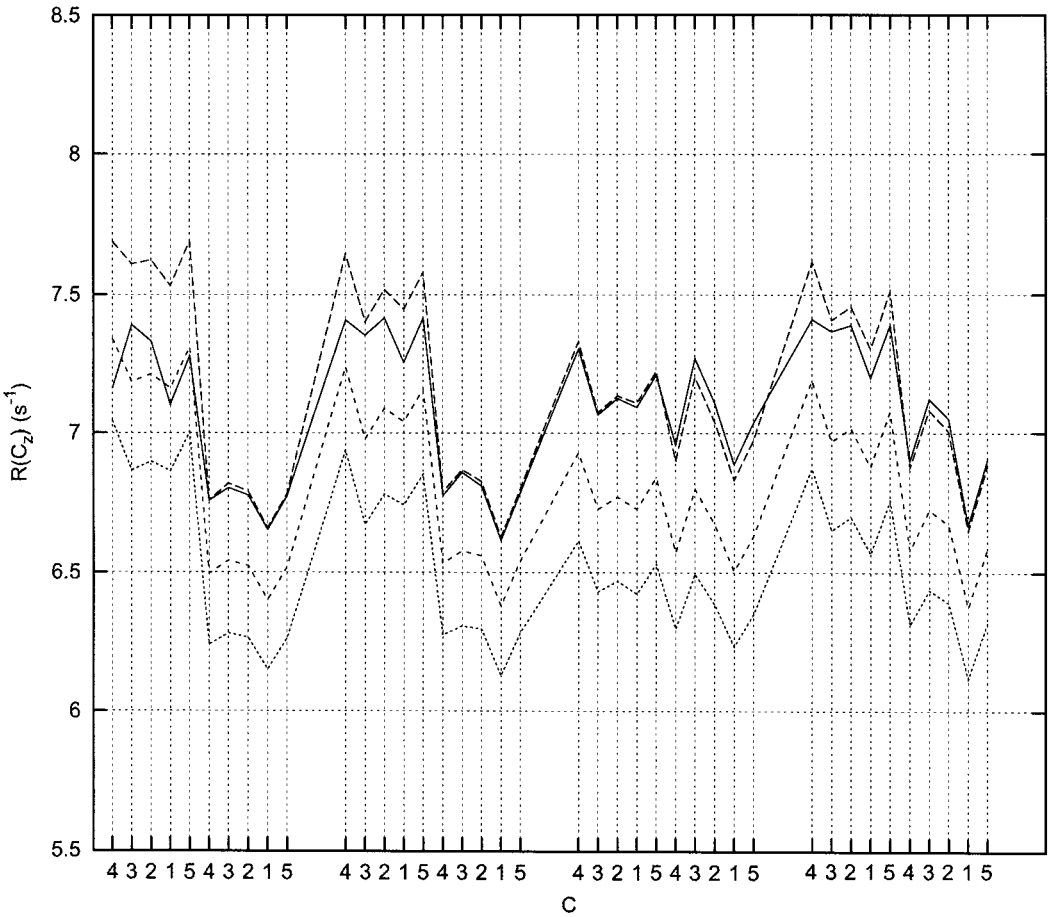

Figure 9. Comparison between ^{13}C relaxivities at 75 MHz calculated with model II, $e = 3$, and different values of α for the rigid starting configuration of the $(UA)_4$ oligomer: $\alpha = 0$ (solid line), $\alpha = 0.25$ (long-dashed line), $\alpha = 0.5$ (short-dashed line), and $\alpha = 0.75$ (dotted line).

sential to understand the probed dynamical pattern. In addition, a flexible molecule, fluctuating according to the MD simulation around the rigid configuration estimated by crystallographic data on the fiber, can provide results close to NMR relaxation experiments while the rigid structure cannot. The contribution of internal rates has been found negligible in the proposed model. It is not clear, however, if this lack of internal contributions may be a limit of the actual modeling that causes the incomplete quantitative agreement with the experimental pattern. Nevertheless, it cannot be discarded either that differences at such a detailed level could be simply due to experimental inaccuracy.

The modeling shows that most of the contributions to the global friction and therefore to the rotational diffusion of the molecule come from the side chains that are mobile and displaced from the main chain (see the schematic representation of friction in Figure 1C).

Modeling the dynamics of hyaluronan oligomers is also a first step for understanding dynamical properties of the macromolecular chain in terms of persistence length, interatomic interactions, bending and twisting fluctuations, solvation, and local rotational diffusion anisotropy.

Acknowledgment. Fruitful discussion with M. Paci and G. Paradossi (Rome) is acknowledged. Financial support has been provided by the Progetto Coordinato "Proprietà dinamiche di oligo e polisaccaridi" Grant CT98-01803.CT03 (CNR) and by COFIN-99 (MURST).

References and Notes

(1) Brant, D. A. *Curr. Opin. Struct. Biol.* **1999**, *9*, 556−562.
(2) Rees, D. *Polysaccharide Shapes*; Chapman & Hall: London, UK 1977.
(3) Burton, B. A.; Brant, D. A. *Biopolymers* **1983**, *22*, 1769−1792.
(4) Perico, A.; Mormino, M.; Urbani, R.; Cesàro, A.; Tylianakis, E.; Dais, P.; Brant, D. A. *J. Phys. Chem. B* **1999**, *103*, 8162−8171.
(5) La Penna, G.; Carbone, P.; Carpentiero, R.; Rapallo, A.; Perico, A. *J. Chem. Phys.* **2001**, *114*, 1876−1886.
(6) La Penna, G.; Fausti, S.; Perico, A.; Ferretti, J. A. *Biopolymers* **2000**, *54*, 89−103.
(7) Fausti, S.; La Penna, G.; Cuniberti, C.; Perico, A. *Mol. Sim.* **2000**, *24*, 307−324; La Penna, G.; Perico, A.; Genest, D. *J. Biomol. Struct. Dyn.* **2000**, *17*, 673−685.
(8) Almond, A.; Brass, A.; Sheehan, J. K. *Glycobiology* **1998**, *8*, 973−980.
(9) Almond, A.; Brass, A.; Sheehan, J. K. *J. Mol. Biol.* **1998**, *284*, 1425−1437.
(10) Scott, J. E.; Heatley, F. *Proc. Natl. Acad. Sci. U.S.A.* **1999**, *96*, 4850−4855.
(11) Allen, M. P.; Tildesley, D. J. *Computer Simulation of Liquids*; Clarendon Press: Oxford, U.K., 1989. Frenkel, D.; Smit, B. *Understanding Molecular Simulation*; Academic Press: San Diego, CA, 1996.
(12) Lipari, G.; Szabo, A. *J. Am. Chem. Soc.* **1982,** *104*, 4546−4570.
(13) Tugarinov, V.; Liang, Z.; Shapiro, Y. E.; Freed, J. H.; Meirovitch, E. *J. Am. Chem. Soc.* **2001**, *123*, 3055−3063.
(14) Withka, J. M.; Swaminathan, S.; Beveridge, D. L.; Bolton, P. H. *J. Am. Chem. Soc.* **1991**, *113*, 5041−5049.
(15) Prompers, J. J.; Scheurer, C.; Brüschweiler, R. *J. Mol. Biol.* **2001**, *305*, 1085−1097.
(16) Prompers, J. J.; Brüschweiler, R. *J. Phys. Chem. B* **2000**, *104*, 11416−11424.
(17) Holmbeck, S. M. A.; Petillo, P. A.; Lerner, L. E. *Biochemistry* **1994**, *33*, 3, 14246−14255.

(18) Cavalieri, F.; Chiessi, E.; Paci, M.; Paradossi, G.; Flaibani, A.; Cesàro, A. *Macromolecules* **2001**, *34*, 99−109.
(19) Cowman, M. K.; Feder-Davis, J.; Hittner, D. M. *Macromolecules* **2001**, *34*, 110−115.
(20) Zwanzig, R. *J. Chem. Phys.* **1974**, *60*, 2717−2720. Perico, A. *Acc. Chem. Res.* **1989**, *22*, 336−342.
(21) Pastor, R. W.; Karplus, M. *J. Phys. Chem.* **1988**, *92*, 2636−2641.
(22) Perico, A.; Pratolongo, R. *Macromolecules* **1998**, *30*, 55958−5969.
(23) La Penna, G.; Pratolongo, R.; Perico, A. *Macromolecules* **1999**, *32*, 506−513.
(24) Peng, J.; Wagner, G. *J. Magn. Res.* **1992**, *98*, 308−332.
(25) Cavanagh, J.; Fairbrother, W. J.; Palmer, A. G., III; Skelton, N. J. *Protein NMR spectroscopy*; Academic Press: San Diego, CA, 1996.
(26) Rose, M. E. *Elementary Theory of Angular Momentum*; John Wiley & Sons: New York, 1957.
(27) Guss, J. M.; Hukins, D. W. L.; Smith, P. J. C.; Winter, W. T.; Arnott, S.; Moorhouse, R.; Rees, D. A. *J. Mol. Biol.* **1975**, *95*, 359−384: entry 3HYA in the Protein Data Bank (http://www.rcsb.org).
(28) Bruccoleri, R. E.; Olafson, B. D.; States, D. J.; Swaminathan, S.; Karplus, M. *J. Comput. Chem.* **1983**, *4*, 187−217.
(29) Ueda, K.; Brady, J. W. *Biopolymers* **1996**, *38*, 461−469.
(30) Jorgensen, W. L.; Chandrasekhar, J.; Madura, J. D.; Impey, R. W.; Klein, M. L. *J. Chem. Phys.* **1983**, *79*, 926−935.
(31) Procacci, P.; Paci, E.; Darden, T.; Marchi, M. *J. Comput. Chem.* **1996**, *18*, 1848−1862.
(32) Procacci, P.; Marchi, M.; Darden, T. *J. Phys. Chem.* **1999**, *100*, 10464−10468.
(33) Tuckerman, M.; Berne, B. J.; Martyna, G. J. *J. Chem. Phys.* **1992**, *97*, 1990−2001.
(34) Essmann, U.; Perera, L.; Berkowitz, M. L.; Darden, T.; Lee, H.; Pedersen, G. L. *J. Chem. Phys.* **1995**, *103*, 8577−8593.
(35) Rotne, J.; Prager, S. J. *J. Chem. Phys.* **1969**, *50*, 4831−4837.
(36) Cremer, D.; Pople, J. A. *J. Am. Chem. Soc.* **1975**, *97*, 1354−1358.
(37) Note that an inversion occurred in some of the data entries of $T_1 = R(C_z)^{-1}$ reported in ref 14. The values must be corrected as follows (values are in seconds). C4 of residue A1, A2, and A3 have $T_1 = 0.34$ (not 0.15), C4 of residue A4 has $T_1 = 0.15$ (not 0.34), C1 of residue U2 and U3 have $T_1 = 0.29$ (not 0.55), C1 of residue U4 has for $\alpha T_1 = 0.50$ (not *n.n*), C1 of residue U4 has for $\beta T_1 = 0.29$ (not 0.50). This correction mainly affects the spikes of C4(A) in Figure 16A of ref 14 and therefore provides some better agreement within the two sets of data reported there.

MA0112220